LATEST MEASUREMENTS OF MAGNETIC NOISE IN THE LHC TUNNEL*

G. Sterbini†, H. Bartosik, M. J. Bednarek, M. Cerqueira Bastos, S. Cettour Cave, S. Kostoglou, M. Martino, M. Praznovsky, A. Radoslavova, G. Trad, D. Valuch, J. Wenninger
European Organization for Nuclear Research, Geneva, Switzerland

Abstract

The magnetic coupling between nearby accelerator rings can introduce unwanted perturbations to beam dynamics, representing a potential concern for future colliders such as the High-Luminosity Large Hadron Collider, or multi-ring facilities such as the Future Circular Collider or the Muon Collider complex. To explore and benchmark this effect, dedicated tests were performed to study the electromagnetic interplay between the SPS and the LHC. Controlled excitations in the SPS were applied while monitoring the response of the beams in the LHC using high-precision instrumentation. Clear signatures of coupling were observed, providing valuable input for the validation of simulation models and for improving the understanding of magnetic field propagation between accelerator infrastructures. In this paper, the results of these measurements are presented and discussed.

INTRODUCTION

The CERN Super Proton Synchrotron (SPS) [1] is a normal-conducting synchrotron with a circumference of approximately 6.9 km. It is located about 75 m above the lowest point of the Large Hadron Collider (LHC) [2, 3] tunnel (Fig. 1), which hosts a superconducting collider with a circumference of about 27 km. The 1.4% slope of the LHC tunnel is visible in Fig. 1.

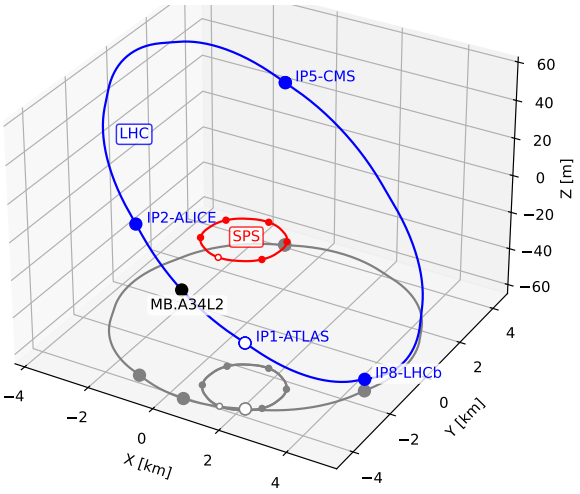

Figure 1: Relative position between SPS and LHC.

Before the LHC era, the tunnel hosted the Large Electron–Positron Collider (LEP) [4]. Several effects affecting LEP energy calibration were investigated in detail [5]. A magnetic coupling between SPS and LEP was already observed [6]: in general, when a current ΔI flows in the SPS ring, a magnetic field can be produced in the LHC tunnel through several mechanisms, for example:

1. a contribution related to the mutual induction voltage between SPS and LHC ($\propto \frac{d\Delta I}{dt}$, the dominant effect reported in [6]);
2. a contribution due to the SPS direct magnetic field ($\propto \Delta I$);
3. a coupling through ground loops [7].

In general, the situation may be further complicated by additional effects on the circuits (e.g., persistent currents in the superconducting cables) and the interplay of the external magnetic field with the active regulation of the involved power supplies (e.g., effect of the magnetic field on the DCCTs readings [8]).

A detailed understanding of the SPS–LHC magnetic coupling is beyond the scope of this study. In this paper we quantify the effect through magnetic measurements in the LHC tunnel and beam-based measurements using LHC beams at 450 GeV, the LHC injection energy.

MEASUREMENT SETUP

The powering and cabling of the SPS main dipoles are designed to cancel the overall SPS magnetic flux. This is not the case for the SPS arc quadrupoles, which belong to two families wired in opposite directions: focusing (QF) and defocusing (QD). Their induced magnetic flux thus cancels only if $I_{QF} = I_{QD}$. For this reason, and to avoid EMC issues with the LHC Quench Protection System [9], the operational currents of the QF and QD circuits are normally kept approximately equal. On 4 September 2025, an ad-hoc measurement was performed by deliberately unbalancing the SPS QF/QD currents up to $|I_{QF} - I_{QD}| = |\Delta I| = 1.7$ kA (Fig. 2) while beams were circulating in the LHC. The magnetic effect of the SPS in the LHC was measured using a

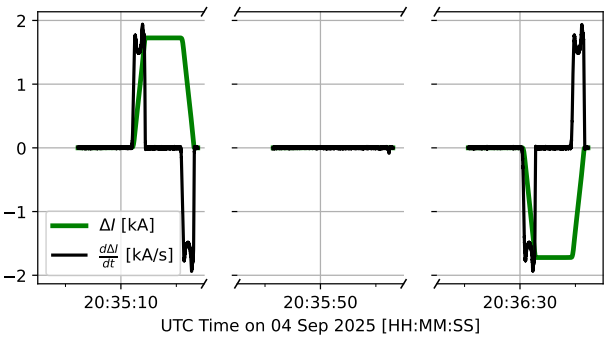

Figure 2: The SPS I_{QF} and I_{QD} powering cycle. The minor x-axis divisions represent 5-seconds intervals.

* Research supported by the HL-LHC project.
† guido.sterbini@cern.ch

three-axis magnetic fluxmeter (Mag-13MSL100 [10]) installed in the middle of LHC Sector 12 (Fig. 3), on top of one of the 1232 main dipoles (MB.A34L2 in Fig. 1). The fluxmeter position defines the origin of the XYZ reference frame used for the magnetic measurements (positive-Z is pointing to IP2-ALICE). Also visible in Fig. 3 are three 70 cm diameter coils used to measure high-frequency magnetic field components, extending the measurement range above 3 kHz (not discussed in this paper). During the measurement, the tunes and the closed orbit of the LHC beams were recorded [11].

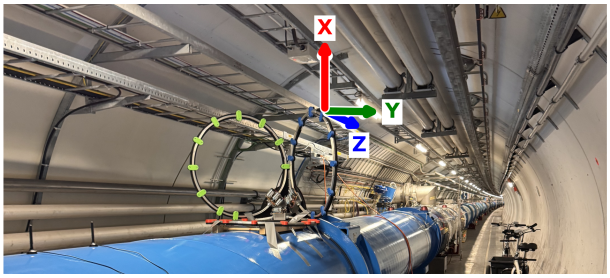

Figure 3: Magnetic measurement setup in the LHC tunnel.

RESULTS

Induced magnetic effect in the LHC tunnel

An example of the measured magnetic fields in the LHC is reported in Fig. 4. Its correlation with the derivative of the difference in the SPS QF and QD current, $d\Delta I/dt$, is very clear. Most of the field is traversal with respect to the LHC beam direction, i.e. lies in the XY plane (Fig. 3). The residual ΔB_z dependence is compatible with the expected precision of the instrument positioning (no survey metrology was adopted), e.g., a roll of 3 degrees would suffice to set $\Delta B_z = 0$, and therefore the main source of the B field is to be attributed to current flowing in the LHC cryostat.

The strongest effect is on B_y with $|\Delta B_y| \approx 10\ \mu$T (peak-to-peak). It is worth noting that the modulus of the earth magnetic field at CERN is expected to be 47 μT [12]. The average magnetic field modulus (28 μT) observed during the measurement is dominated by the magnetization of the ferromagnetic material (mainly the magnet iron yoke) and main dipole fringe field.

The singular values (SV) analysis [13, 14] of the three magnetic field components reveals that the signals are dominated by the first mode, capturing $\frac{SV_1^2}{\sum_i SV_i^2} = 98.78\%$ of the total variance (Fig. 5). Notably, despite the first mode being strongly dominated by the LHC-SPS mutual inductance, non-SPS driven excitations are also contributing to the same mode (e.g., B_y low-amplitude oscillations between 20:40 and 20:43). This proves the complexity of the LHC magnetic environment and, at the same time, the potential of the measurement setup to better understand the effects on the beam, as we will analyze in the following subsection.

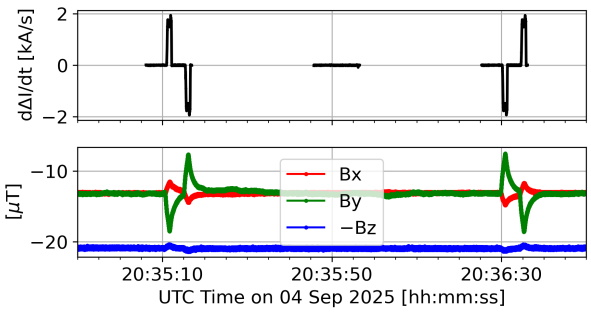

Figure 4: Measured magnetic fields in the LHC Tunnel.

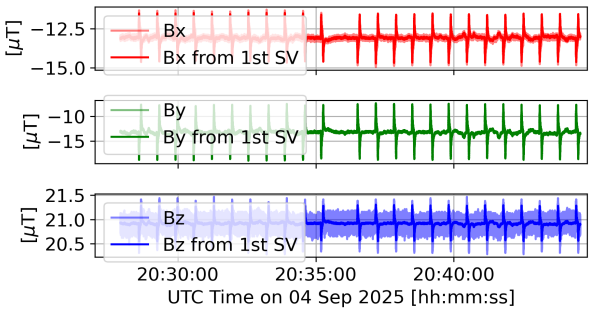

Figure 5: Filtering only the first singular value components.

The voltage signals on the MB.A34L2 dipole were also monitored when unbalancing the SPS QF/QD circuits, but no induced signal could be observed. It is suggested to test, during the next LHC long stop, larger loops as done in LEP with the compensating QF-QD loop [6] [15], e.g., measuring the voltage between the adjacent magnets MB.A34L2 and MB.B34L2 as done in 26 June 2025 [16].

Induced effect on the LHC beams

The beam tunes were affected by the SPS excitation, as shown in Fig. 6 (LHC Fill 11029, injection energy plateau).

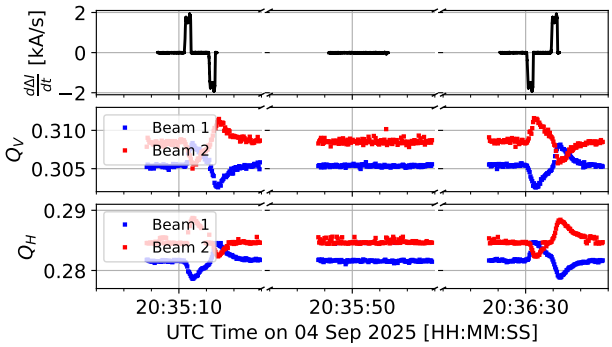

Figure 6: Tune measurement in the LHC during excitation of the SPS QF/QD circuits.

The tune measurement was performed without kicker excitation using the Base Band tune measurement system [17]. A single bunch circulated with an intensity of approximately 0.93×10^{10} p, and the arc octupoles were switched off. Reconstruction of the beam tune using the LHC transverse feedback pickups [18] did not provide a better signal.

The peak-to-peak tune variation is approximately 6×10^{-3}, with $\Delta Q_x|_{B1} \simeq -\Delta Q_y|_{B1} \simeq -\Delta Q_x|_{B2} \simeq \Delta Q_y|_{B2}$. The chromaticity was set to 5 units for both beams and planes.

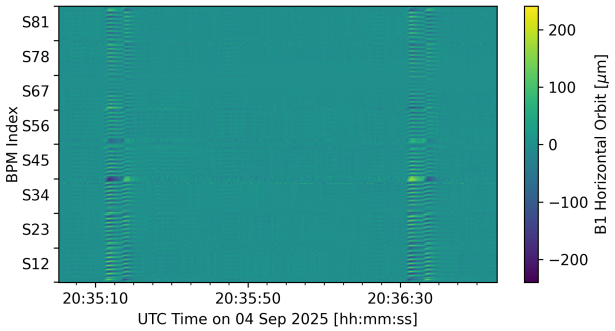

Figure 7: Closed-orbit variation in Beam 1 horizontal plane. On the y-axis the BPMs are shown for each LHC sector.

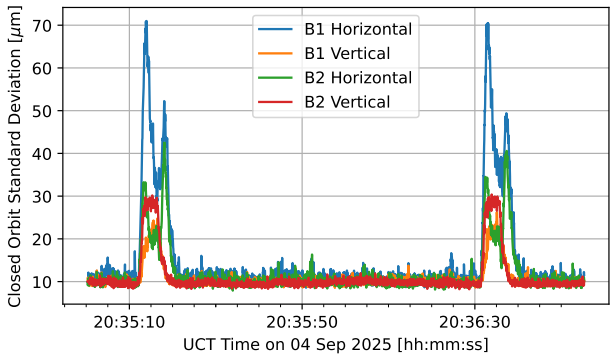

Figure 8: Closed-orbits standard deviation.

The observed tune pattern is therefore not compatible with a momentum-induced effect, which would produce identical tune shifts in both planes, and instead points to a distributed perturbation along the machine.

Closed-orbit measurements acquired at 25 Hz were available for both beams and planes, and a clear orbit response to the SPS excitation was observed. Figure 7 shows the measurement for Beam 1 in the horizontal plane. The plot reports the signals from the 542 LHC BPMs versus time after subtraction of the average closed orbit. A peak oscillation of approximately ±200 μm is observed during the SPS QF/QD excitation.

The noise level, estimated from the standard deviation of the BPM signals, is about 10 μm for both beams and planes (Fig. 8). Nevertheless, the SPS-induced orbit variation reaches up to 70 μm rms.

Given the stronger signals, the following analysis focuses on the horizontal plane. Filtering the first three SV modes of the BPM signals captures 72.0% and 50.2% of the total signal variance for Beam 1 and Beam 2, respectively. These filtered signals are used to reconstruct the effective kicks along the machine.

To reconstruct the distributed perturbation, 10 000 evenly-spaced effective kicks were simulated along each beam line. The RMS of the reconstructed kicks was studied as a function of the number of SVs used to pseudoinvert the response matrix (Fig. 9) [19]. Using 190 SVs (out of 542) yields the solution shown in Fig. 10.

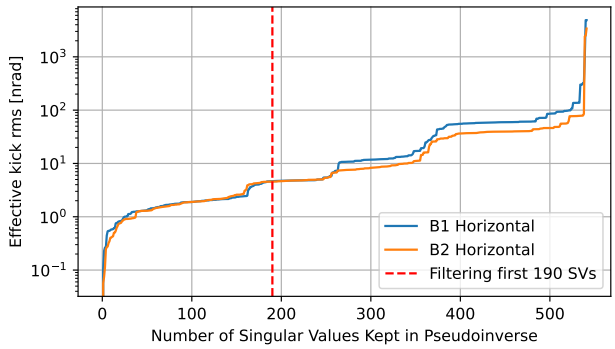

Figure 9: RMS of reconstructed kicks vs the number of SVs used in the pseudoinverse of the response matrix.

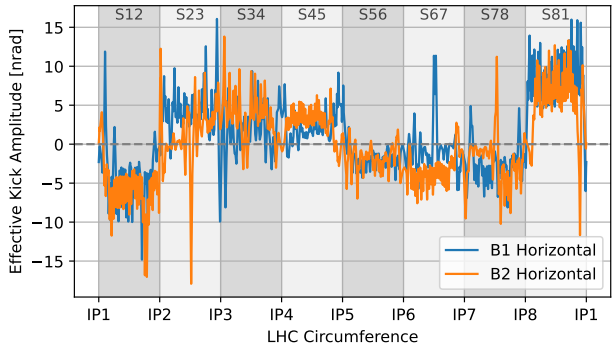

Figure 10: Horizontal effective kicks for Beam 1 and 2.

Despite the high frequency jitter, several features clearly emerge: (1) the effective kicks of the two beams are strongly correlated (it is to be noted that the SPS induced field in the two apertures is inverted); (2) they oscillate around sector-dependent average values along the eight LHC sectors; (3) a change of sign of the sector average occurs when the beam transitions between the internal and external apertures (e.g. at IP1–ATLAS, IP2–ALICE, IP5–CMS, and IP8–LHCb); (4) Sectors 12 and 81, which are closest to the SPS, exhibit larger average effective kicks than the other sectors.

CONCLUSIONS

The observations collected in this paper show (1) the maturity of the diagnostic to analyze subtle effects like the coupling between the SPS and the LHC and (2) point to a two-aperture/single-sector effect.

For the authors, similar approaches can be adopted during the HL-LHC string [20] test and the optimization of future lepton colliders (e.g. FCC-ee [21] and LEP3 [22]), where the main collider shares the same tunnel with a fast-cycling booster ring.

ACKNOWLEDGMENTS

The authors are indebted to P. Bélanger, R. De Maria, A. Fornara and K. Li for the inspiring discussions, and to the CERN LHC and SPS operation teams for the invaluable support during the measurement campaign.

REFERENCES

[1] J. Coupard *et al.*, *LHC Injectors Upgrade, Technical Design Report*, J. Coupard, Ed. 2014. doi:10.17181/CERN.7NHR.6HGC

[2] O. S. Brüning *et al.*, "LHC Design Report", CERN, Geneva, Rep., 2004. doi:10.5170/CERN-2004-003-V-1

[3] O. Aberle *et al.*, "High-Luminosity Large Hadron Collider (HL-LHC): Technical design report", CERN, Geneva, Rep., 2020. doi:10.23731/CYRM-2020-0010

[4] "LEP design report", CERN, Geneva, Rep., 1984. doi:10.17181/CERN.AXZH.185L

[5] L. Arnaudon *et al.*, "Accurate determination of the LEP beam energy by resonant depolarization", *Zeitschrift fr Physik C Particles and Fields*, vol. 66, no. 1-2, pp. 45–62, Mar. 1995. doi:10.1007/BF01496579

[6] O. E. Berrig *et al.*, "Magnetic Coupling Between SPS And LEP - CERN Document Server", CERN, Geneva, Rep. CERN-LEP-Performance-Note-54, 1991. https://cds.cern.ch/record/443417/

[7] G. Brun *et al.*, "A newly observed Effect affects the LEP Beam Energy", 1996. https://cds.cern.ch/record/309231

[8] M. Sugiura and T. K. M. Tobiyamat, "Influence of External Magnetic Field on Beam DCCT". https://www.pasj.jp/web_publish/sast1993/26PB27.pdf

[9] K. Dahlerup-Petersen, F. Rodriguez-Mateos, R. Schmidt, and F. Sonnemann, "Energy extraction for the LHC superconducting circuits", *Conf. Proc. C*, vol. 0106181, pp. 3448–3450, 2001.

[10] "Mag-13® three-axis magnetic field sensors", https://www.bartingtondownloads.com/wp-content/uploads/DS3143.pdf (visited on 03/03/2026),

[11] "MD16063 gitlab repository", en, Mar. 2026, https://gitlab.cern.ch/abpcomputing/sandbox/md16063 (visited on 03/06/2026),

[12] "pyIGRF: IGRF-14 Model by Python", https://github.com/zzyztyy/pyIGRF (visited on 03/03/2026),

[13] S. M. Kay, "Fundamentals of statistical signal processing. 1: Estimation theory", eng, in 20. pr, Num Pages: 595, Upper Saddle River, NJ: Prentice Hall PTR, 2013, ISBN: 978-0-13-345711-7,

[14] I. Selesnick, "Least Squares with Examples in Signal Processing". https://eeweb.engineering.nyu.edu/iselesni/lecture_notes/least_squares/least_squares_SP.pdf

[15] P. Collier, "Effect of QF-QD compensation on LEP beam energy", Geneva, 1993, https://cds.cern.ch/record/702886,

[16] G. Sterbini, "Summary of EPC measurements", Oct. 2025. doi:10.5281/ZENODO.18978239

[17] M. Gasior and R. Jones, "High Sensitivity Tune Measurement by Direct Diode Detection", 2005. https://cds.cern.ch/record/895142

[18] M. E. Söderén and D. Valuch, "ADTOBSBOX to catch instabilities", 2020, doi:10.23732/CYRCP-2020-009.154,

[19] Y. Chung, G. Decker, and K. Evans, "Closed Orbit Correction Using Singular Value Decomposition of the Response Matrix", 1993. https://cds.cern.ch/record/901051

[20] S. Yammine *et al.*, "Experimental Program of the HL-LHC Inner Triplet String Test at CERN", *IEEE Transactions on Applied Superconductivity*, vol. 34, no. 5, pp. 1–5, Aug. 2024. doi:10.1109/TASC.2023.3349356

[21] A. Abada *et al.*, "FCC-ee: The Lepton Collider", *The European Physical Journal Special Topics*, vol. 228, no. 2, pp. 261–623, Jun. 2019. doi:10.1140/epjst/e2019-900045-4

[22] C. Anastopoulos *et al.*, "LEP3: A High-Luminosity e+e- Higgs and ElectroweakFactory in the LHC Tunnel", Nov. 2025, doi:10.48550/arXiv.2504.00541,